

## ANALYSIS OF INFRARED TEMPERATURE MEASUREMENT FOR FLUE GAS SHIELDING METAL SURFACE USING SOURCE MULTI-FLUX METHOD

by

**Wei WANG<sup>a\*</sup>, Jie-Dong LIN<sup>a</sup>, Wan-Li ZHONG<sup>a</sup>, Biao ZHANG<sup>b\*</sup>,  
Chuan-Long XU<sup>b</sup>, and Hui DING<sup>b</sup>**

<sup>a</sup> Electric Power Research Institute of Guangdong Power Grid Co., Ltd., Guangzhou, China

<sup>b</sup> School of Energy and Environment, Southeast University, Nanjing, China

Original scientific paper

<https://doi.org/10.2298/TSCI150904067W>

*The infrared temperature measurement technique has been applied in various fields with the development of charge coupled device. In the problem of metal surface temperature measurement, if the surface is covered by participating media, the traditional infrared temperature measurement technique will lead to intolerable measurement errors. In this work, the infrared temperature measurement problem was solved by the source multi-flux method. On this base, the impact of the flue gas thickness and surface temperature on the apparent temperature measured by the charge coupled device was analyzed. Furthermore, the corresponding experimental system was set up. And the experimental results were found to have a good agreement with the simulated results. Finally, the idea of modification for the infrared temperature measurement by inverse method was proposed.*

**Key words:** *infrared temperature measurement, source multi-flux method, radiative heat transfer, impact analysis*

### Introduction

The surface temperature of superheater is a very important monitor parameter in a power plant boiler system. The stability and continuity of the online temperature measurement is the basic premise to achieve security control of the superheater [1]. When the temperature of the superheater is high, it will accelerate the creep of metal materials. This will make the superheater, steam pipeline and high pressure turbine section generate additional thermal stress. Then the lifespan of the equipment will be cut. When the superheater is severe over-temperature, the pipeline can result in blast, which seriously affect the long term operation of the boiler [2]. Therefore, in the development trend of large-capacity and high parameters in thermal power units, effective monitoring of the security status of the key components and achieving material life assessment are urgent problems to be solved during the safe and stable operation of the boiler.

For the surface temperature measurement, practical applications generally use contact measurement methods, such as thermocouple, thermal resistance, as well as temperature thermometer [3-5]. In the current superheater temperature measurement methods, thermocou-

---

\* Corresponding author's, e-mail: [wwangcn@163.com](mailto:wwangcn@163.com), [zhangbiao@seu.edu.cn](mailto:zhangbiao@seu.edu.cn)

ple is widely used in power station. In order to improve the measurement accuracy and reliability, a variety of thermocouple installation methods have been proposed, such as embedding method, capping method, water cooling lead method, metal spraying method [6, 7]. Thermocouple temperature measurement belongs to contact temperature measurement method. Though its accuracy is high, it impacts the original temperature field of the object, and it is easy to cause damage in harsh condition. In addition, the number of layout of the thermocouple is often limited. Thus it is unable to obtain the entire temperature field distribution of the steam pipe [8].

In contrast, radiative temperature measurement belongs to non-contact temperature measurement method. It can overcome the previous drawbacks, and has drawn more and more attention in recent years. The fundamental principles of the radiative temperature measurement are Planck's law, Wien's law, and Stefan-Boltzmann law [9, 10]. However, due to the impact of the spectral emissivity, the measured temperature is not the real temperature of the object. There are radiation temperature, brightness temperature and colorimetric temperature for different types of detectors. It needs emissivity correction to get the real temperature. Methods used in the past mainly contain black-body approximation method, auxiliary source method, and polarization method [11-14]. With the rapid development of the radiative temperature measurement technology, there have been some radiative thermometers with very high accuracy, especially infrared camera. It can distinguish 0.01 °C or less in surface temperature measurement [15]. To measure surface temperature of superheater by radiative temperature measurement method, the impact of the surface emissivity, medium radiative parameters and complex flow field must be considered. Since the radiative signal obtained by the detector is the overall radiative signal from surface and medium, it needs to establish a mathematical model to explore the relationship between surface temperature and detected signal. And then find a suitable algorithm to obtain the real surface temperature.

In this paper, the infrared temperature measurement problem was solved by the source multi-flux method. Then, the impact of the flue gas thickness and surface temperature on the apparent temperature measured by the charge coupled device (CCD) was analyzed. Furthermore, the corresponding experimental system was set-up. Finally, the idea of modification for the infrared temperature measurement by inverse method was proposed.

### Measurement theory

Infrared temperature measurement method is to use the radiative energy of the measured surface received by an infrared CCD camera to determine the object temperature. According to the principle of infrared CCD camera temperature measurement, the effective radiation detected by infrared CCD camera contains three parts, namely, the emission of the object itself, the reflection of the environment, and the participation of the media. The schematic of the effective radiation in infrared temperature measurement is shown in fig. 1. Infrared CCD camera typically operates in several bands, such as 2-5 μm and 8-13 μm. For monochromatic radiative temperature measurement method, a filter slice, which allows only a narrow band of light to pass through, is needed to add in the lens. The detector can convert the radiative signal to an electrical signal, which is proportional to energy. The universal basic formula of the infrared temperature measurement is [16]:

$$V = Ad^{-2} \{ \tau_{\lambda} [ \varepsilon_{\lambda, \text{obj}} E_{\text{obj}} + (1 - \varepsilon_{\lambda, \text{obj}}) E_{\text{refl}} ] + \varepsilon_{\lambda, \text{med}} E_{\text{med}} \} \quad (1)$$

where  $V$  is the voltage signal of the detector,  $A$  – the viewing area of the target corresponding to minimum space angle of the CCD camera,  $d$  – the distance between the target and the camera,  $\tau_\lambda$  – the transmittance of the media at wavelength  $\lambda$ ,  $\varepsilon_{\lambda, \text{obj}}$ , and  $\varepsilon_{\lambda, \text{med}}$  – the spectral emissivity of the target and equivalent spectral emissivity of the media, respectively,  $E_{\text{obj}}$  – the energy emitting from the surface of the target,  $E_{\text{refl}}$  – the projection energy from the nearby surface to the target, and  $E_{\text{med}}$  – the emitting energy of the media.

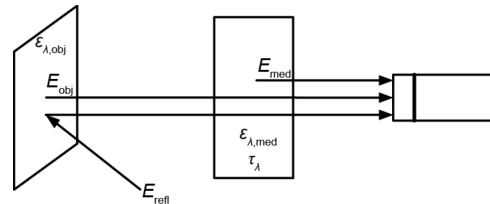


Figure 1. The schematic of the effective radiation in infrared temperature measurement

The self-radiation can be defined by Planck's law, which is the theoretical basis of infrared temperature measurement. It reveals the black-body radiation energy distribution at different temperatures and different wavelengths. The mathematical expression is:

$$E_{b\lambda} = \frac{c_1 \lambda^{-5}}{e^{c_2/\lambda T} - 1} \quad (2)$$

where  $E_{b\lambda}$  is the black-body spectrum radiation. The  $c_1$  and  $c_2$  denote the first and second radiation constants, respectively,  $c_1 = 3.7415 \cdot 10^{-12} \text{ W/cm}^2$  and  $c_2 = 1.4388 \text{ cmK}$ ,  $\lambda$  is the wavelength of the spectrum radiation, and  $T$  – the absolute temperature of the black-body.

### Measurement system

The experimental rig of infrared temperature measurement for flue gas shielding surface is shown in fig. 2. The measurement rig consists of an infrared CCD camera, infrared lens, vibrating screen, and muffle furnace. The infrared CCD is chosen as MAG62, whose frame rate is 50 Hz. Its detector type is uncooled focal plane. It contains  $640 \times 480$  pixel. The size of every pixel is about  $17 \mu\text{m}$ . The model of the infrared lens, whose material is chosen as Ge, is MAGNITY C f25F1. In order to reduce the influence of the water vapor and  $\text{CO}_2$  on radiative transfer, a filter whose center wavelength is  $10 \mu\text{m}$ , is set in the infrared lens. The vibrating screen is placed between the lens and furnace. It is used to simulate the influence of fly ash on infrared temperature measurement. A circular viewing area is set at the axial of the vibrating screen. The width of the vibrating screen can be adjusted. In the experiment, it is set as 5, 10, 15, 20, 25, and 30 mm in sequence to simulate the influence of the thickness of the flue gas. The model of the muffle furnace, with a diameter of 100 mm hole in the center of the side cover, is SX2-4-10. Its rated power is 4 kW. The temperature range is from room temper-

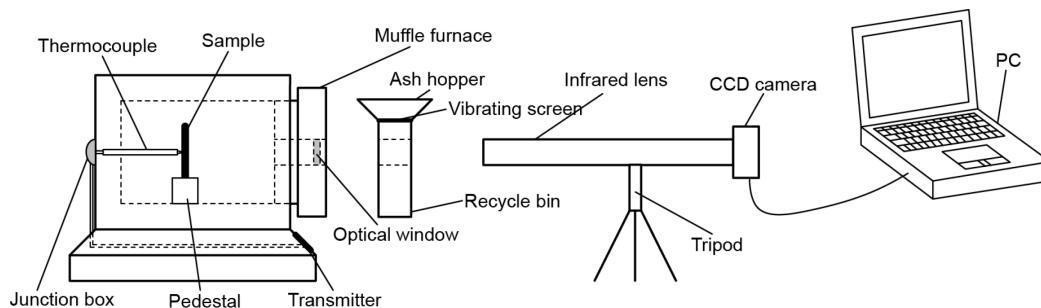


Figure 2. The schematic of experimental rig

ature to 1000 °C. The material of the sample is set as 15 CrMo, the same as the superheater. The material of the optical window is BaF, which has a high transmittance at 10 μm. Its transmittance curve is shown in fig. 3.

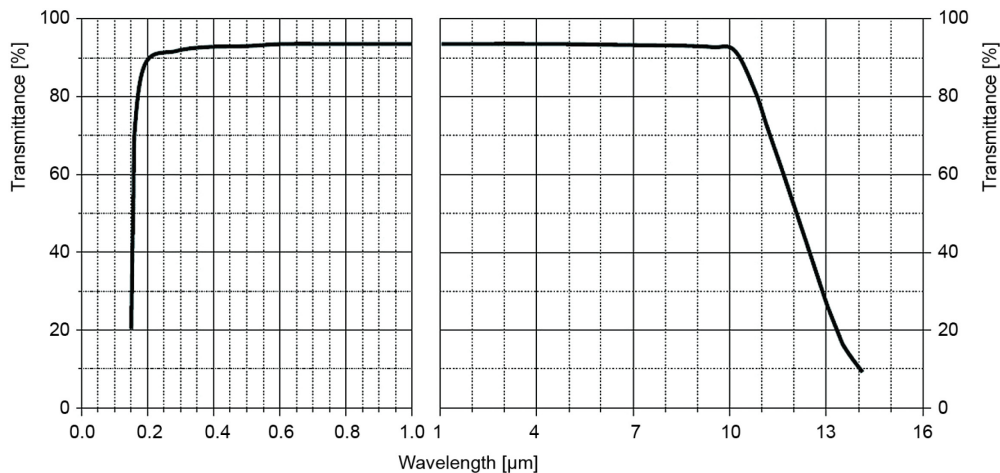


Figure 3. The transmittance curve of BaF

## Results and discussion

### Analytical method

Source multi-flux method is a fast and accurate method based on the finite volume method (FVM) for solving any direction radiative intensity within a semi-transparent medium, which takes into account computational efficiency and accuracy, and can reach close to the accuracy of the Monte Carlo method (MCM). It also has the computational efficiency and broad applicability of FVM and has important theoretical and practical value on infrared warning, combustion diagnostics and remote sensing in directed radiation detection [17].

Due to the extremely high propagation velocity of the radiative energy, the time it takes to reach radiative equilibrium is much less than that of the temperature response. It belongs to a steady radiative transfer problem. The steady-state radiative transfer problems of the uniform refractive index medium can be described with the steady-state radiative transfer equation:

$$\frac{dI(\lambda, \mathbf{r}, \boldsymbol{\Omega})}{ds} = -\beta I(\lambda, \mathbf{r}, \boldsymbol{\Omega}) + \kappa I_b(\lambda, \mathbf{r}) + \frac{\sigma_s}{4\pi} \int_{4\pi} I(\lambda, \mathbf{r}, \boldsymbol{\Omega}') \Phi(\boldsymbol{\Omega}, \boldsymbol{\Omega}') d\boldsymbol{\Omega}' \quad (3)$$

where  $n$  is the refractive index of the medium,  $I(\lambda, \mathbf{r}, \boldsymbol{\Omega})$  – the radiative intensity in the position at  $\mathbf{r}$ , the direction for  $\boldsymbol{\Omega}$ , and the wavelength for  $\lambda$ ,  $I_b(\lambda, \mathbf{r})$  – the radiative intensity of the medium,  $s$  – the distance in direction  $\boldsymbol{\Omega}$ ,  $\beta$ ,  $\kappa$  and  $\sigma_s$  represent the extinction, absorption and scattering coefficients, respectively,  $\Phi(\boldsymbol{\Omega}, \boldsymbol{\Omega}')$  – the scattering phase function,  $\boldsymbol{\Omega}'$  – the incident direction, and  $\boldsymbol{\Omega}$  – the scattering direction.

Then the generalized source term  $S(\lambda, \mathbf{r}, \boldsymbol{\Omega})$  can be defined as the sum of emission enhancement items and scattering enhancement items. It is described as [18]:

$$S(\lambda, \mathbf{r}, \boldsymbol{\Omega}) = \kappa I_b(\lambda, \mathbf{r}) + \frac{\sigma_s}{4\pi} \int_{4\pi} I(\lambda, \mathbf{r}, \boldsymbol{\Omega}') \Phi(\boldsymbol{\Omega}, \boldsymbol{\Omega}') d\Omega' \quad (4)$$

The radiative transfer equation can be written in the following form:

$$\frac{dI(\lambda, \mathbf{r}, \boldsymbol{\Omega})}{ds} = -\beta I(\lambda, \mathbf{r}, \boldsymbol{\Omega}) + S(\lambda, \mathbf{r}, \boldsymbol{\Omega}) \quad (5)$$

Furthermore, eq. (3) can be transformed into the form of separation of variables:

$$\frac{d}{ds} [I(\lambda, \mathbf{r}, \boldsymbol{\Omega}) \exp(\beta s)] = S(\lambda, \mathbf{r}, \boldsymbol{\Omega}) \exp(\beta s) \quad (6)$$

The following formula can be obtained by integrating the control body on both sides of the eq. (4):

$$\int_0^{\Delta s} d[I(\lambda, \mathbf{r}, \boldsymbol{\Omega}) \exp(\beta s)] = \int_0^{\Delta s} S(\lambda, \mathbf{r}, \boldsymbol{\Omega}) \exp(\beta s) ds \quad (7)$$

By simplifying eq. (5) we will get a recurrence formula:

$$I(\lambda, \mathbf{r}_B, \boldsymbol{\Omega}) = I(\lambda, \mathbf{r}_A, \boldsymbol{\Omega}) \exp(-\beta \Delta s) + \frac{S(\lambda, \mathbf{r}_p, \boldsymbol{\Omega})}{\beta [1 - \exp(-\beta \Delta s)]} \quad (8)$$

This recurrence formula is applicable in any direction. Therefore, when calculating the medium radiative intensity  $I(\lambda, \mathbf{r}_p, \boldsymbol{\Omega})$  at any position  $\mathbf{r}_p$  in any direction  $\boldsymbol{\Omega}$ , as shown in fig. 4, the radiative intensity of any point along this direction  $I(\lambda, \mathbf{r}_x, \boldsymbol{\Omega})$ , the generalized source term of the control volumes between these two points  $S(\lambda, \mathbf{r}_i, \boldsymbol{\Omega})$ , and the distance in these volumes  $\Delta s_i$  should be known. In the infrared surface temperature measurement model, the radiative intensity, or the temperature of the surface can be obtained by the intensity of the detector sensor using eq. (8).

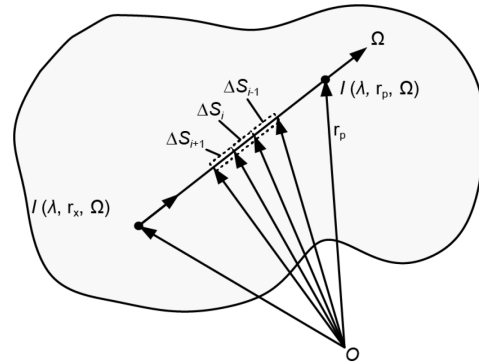
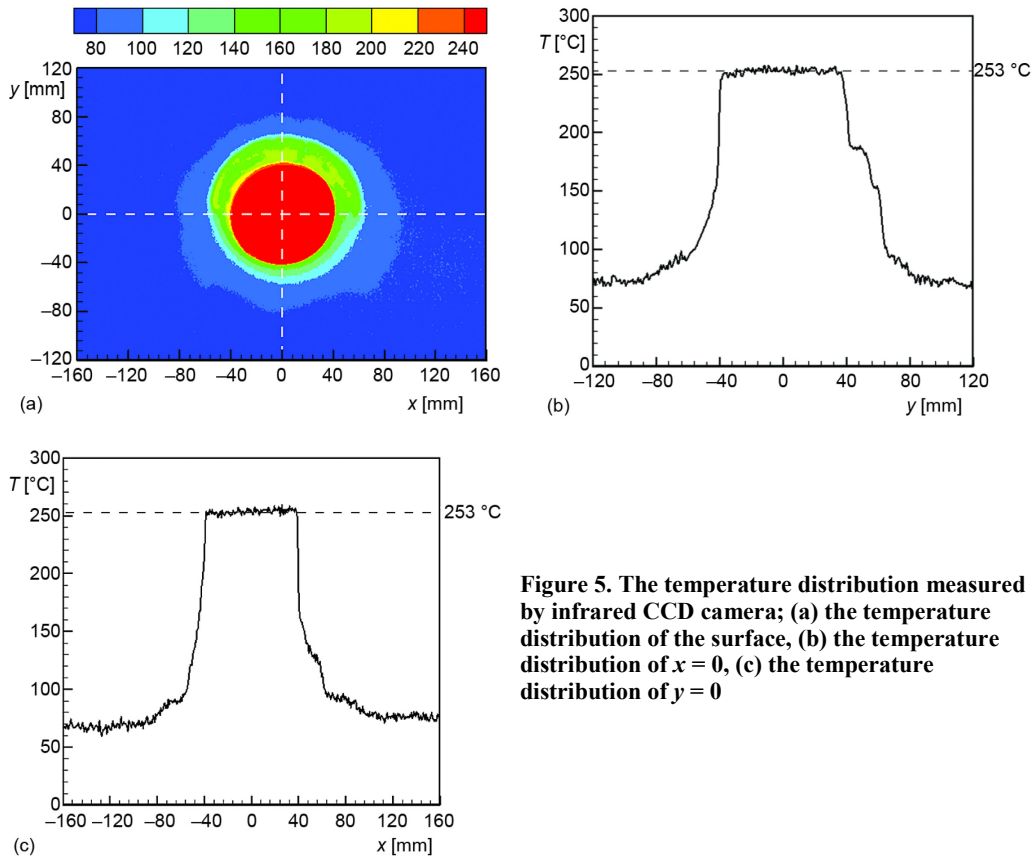


Figure 4. The schematic of arbitrary directional radiative intensity computation

#### Analysis model

Infrared CCD camera used in the experiment has been calibrated at the factory. But because of the different laboratory conditions, the camera needs a secondary calibration. The black-body furnace used in the experiment is produced by AMETEK Company Berwyn, Penn., USA. The type of the black-body is chosen as LANDCAL R1500T. Its temperature resolution is 1 °C. The stability is less than  $\leq \pm 1$  K, over 30 minutes at set time. The heating rate can achieves 1450 °C within 30 minutes. The emissivity is close to 0.99. The temperature of the muffle furnace was set as 250 °C, and stably working for half an hour. When there is no ash in the ash hopper, the temperature distribution of the sample surface is measured by infrared CCD camera, which has been secondly calibrated by the black-body furnace. The infrared image is shown in fig. 5(a). Figures 5(b) and 5(c) show the temperature distribution of  $x = 0$  and  $y = 0$ . It can be seen that the surface temperature distributes uniformly and the average



**Figure 5.** The temperature distribution measured by infrared CCD camera; (a) the temperature distribution of the surface, (b) the temperature distribution of  $x = 0$ , (c) the temperature distribution of  $y = 0$

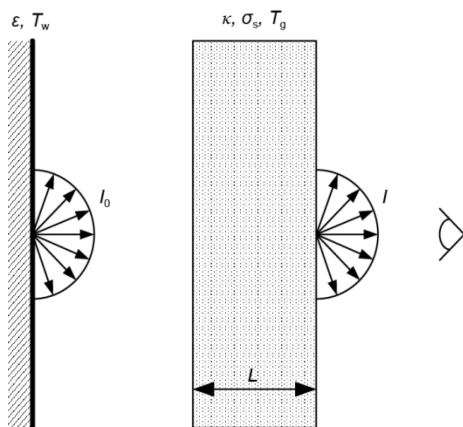


**Figure 6.** Schematic of the infrared temperature measurement for 1-D plane-parallel slab model

was considered as isotropic scattering. The temperature of the muffle was 527 °C and the

temperature is 253 °C which is basically identical to the preset temperature 250 °C. The difference is mainly caused by the thermal inertia of the muffle furnace. As the temperature distribution is basically uniform, the infrared temperature measurement model can be regarded as a 1-D plane-parallel slab, fig. 6.

#### Impact analysis

The influence of vapor and  $\text{CO}_2$  were removed effectively as the central wavelength was chosen as 10  $\mu\text{m}$ . Therefore, in the region without ashes the attenuation of radiative transfer can be neglected. The temperature of the ash was set as 27 °C. The absorption and scattering coefficients under the constant velocity were set as 45.6  $\text{m}^{-1}$  and 3.5  $\text{m}^{-1}$ , respectively. The ash

width of the vibrating screen varied between 1 mm and 50 mm. The surface infrared radiation energy which was absorbed and scattered by the ash and then detected by the detector can be calculated by the source multi-flux method, fig. 7. It can be seen that the measured apparent temperature decreases exponentially with the increasing of the thickness of the ash.

The width of the vibrating screen was set as 20 mm. The same ash was applied and the velocity was constant, which means the absorption, scattering coefficients, and the temperature of the ash were constant. The temperature of the muffle varied between 27 °C and 527 °C. The apparent temperature calculated by the source multi-flux method is shown in fig. 8. It can be seen that the measured apparent temperature increases exponentially with the increasing of the muffle temperature.

The muffle temperature was set as 250 °C. The width of the vibrating screen was chosen as 5, 10, 15, 20, 25, and 30 mm. The experimental apparent temperature is shown in fig. 9. The apparent temperature calculated by source multi-flux method was set as the reference temperature. It can be seen that the measuring temperature and the calculated temperature match well with a maximum error of 9.2 °C. If the apparent temperature was applied as measured value and the source multi-flux method was used as the direct model, the real temperature of the surface can be estimated, which can be applied to the temperature online measuring field of the utility boiler superheater.

### Conclusions

The source multi-flux method was applied to the infrared temperature measurement of the surface covered by flue gas. On this basis, the impact of the flue gas thickness and surface temperature on the apparent temperature was analyzed. Moreover, the measured apparent temperature decreases exponentially with the increasing of the thickness of the ash and increases exponentially with the increasing of the muffle temperature, which were also verified by experiment. Further simulation results can

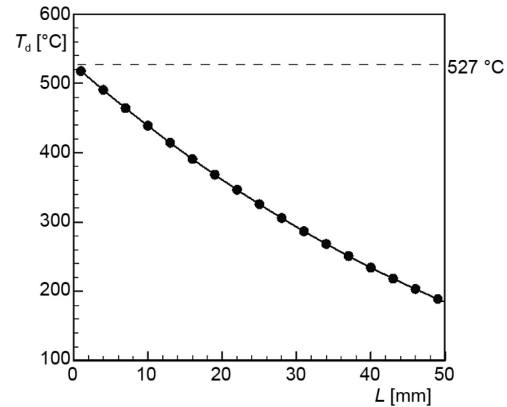


Figure 7. The apparent temperature vs. the width of the vibrating screen

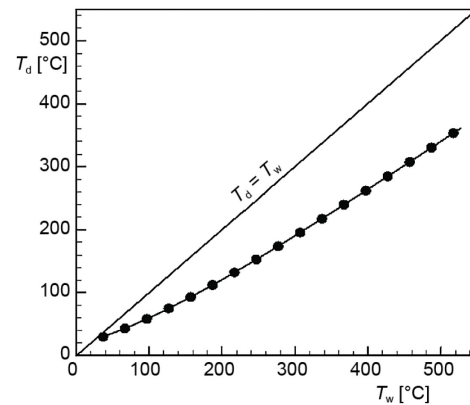


Figure 8. The apparent temperature vs. the set temperature of the muffle furnace

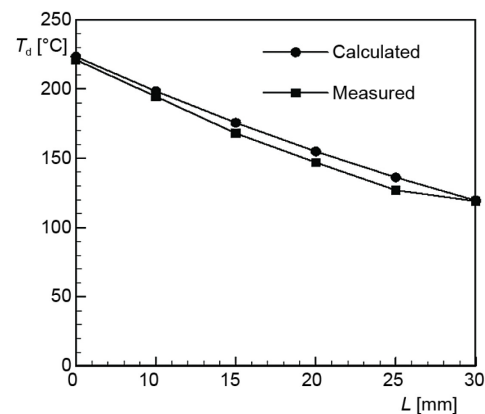


Figure 9. Comparison of the calculated and measured temperatures at different widths of the vibrating screen

be applied to modify the measured apparent temperature. Then the true temperature of the surface covered by flue gas can be obtained which can be applied to the temperature online measuring field of the utility boiler superheater.

### Acknowledgment

This work was supported by Science and Technology Program of China Southern Power Grid Co., Ltd. (No. K- GD2013-0497) and by Special Fund for Basic Research on Scientific Instruments of the National Natural Science Foundation of China (No. 51327803).

### Nomenclature

$A$	– viewing area, [m <sup>2</sup> ]	$\Phi$	– scattering phase function, [–]
$c_1$	– first radiation constants (= $3.7415 \cdot 10^{-12}$ ), [Wcm <sup>-2</sup> ]	$\kappa$	– absorption coefficient, [m <sup>-1</sup> ]
$c_2$	– second radiation constants (= 1.4388), [cmK]	$\lambda$	– wavelength, [μm]
$d$	– working distance, [m]	$\sigma_s$	– scattering coefficient, [m <sup>-1</sup> ]
$E$	– energy, [Wm <sup>-2</sup> ]	$\tau$	– transmittance, [–]
$I$	– radiative intensity, [Wm <sup>-2</sup> sr <sup>-1</sup> ]	$\Omega, \Omega'$	– incoming and outgoing direction vectors, [–]
$L$	– length of the media, [m]	<i>Subscripts</i>	
$\mathbf{r}$	– position vector, [m]	b	– black-body
$S$	– source, [Wm <sup>-3</sup> sr <sup>-1</sup> ]	d	– detector
$s$	– distance in a direction, [m]	g	– gas
$T$	– temperature, [K]	med	– media
$V$	– voltage signal, [Wm <sup>-2</sup> ]	obj	– object
<i>Greek symbols</i>		refl	– reflectance
$\beta$	– extinction coefficient, [m <sup>-1</sup> ]	w	– wall
$\varepsilon$	– emissivity, [–]		

### References

- [1] Yin, C., et al. Investigation of the Flow, Combustion, Heat-Transfer and Emissions from A 609mw Utility Tangentially Fired Pulverized-Coal Boiler, *Fuel*, 81 (2002), 6, pp. 997-1006
- [2] Ehyaei, M. A., Estimation of Condensate Mass Flow Rate During Purging Time in Heat Recovery Steam Generator of Combined Cycle Power Plant, *Thermal Science*, 18 (2014), 4, pp. 1389-1397
- [3] AlWaaly, A. A. Y., et al., Effects of Thermocouple Electrical Insulation on the Measurement of Surface Temperature, *Applied Thermal Engineering*, 89 (2015), Oct., pp. 421-431
- [4] Qi, H., et al., Inversion of Particle Size Distribution by Spectral Extinction Technique Using the Attractive and Repulsive Particle Swarm Optimization Algorithm, *Thermal Science*, 19 (2015), 6, pp. 2151-2160
- [5] Childs, P. R. N., et al., Review of Temperature Measurement. *Review of Scientific Instruments*, 71 (2000), 8, pp. 2959-2978
- [6] Svantner, M., et al., Non-Contact Charge Temperature Measurement on Industrial Continuous Furnaces and Steel Charge Emissivity Analysis, *Infrared Physics & Technology*, 61 (2013), Nov., pp. 20-26
- [7] Li, D. I., Wells, M. A., Effect of Subsurface Thermocouple Installation on the Discrepancy of the Measured Thermal History and Predicted Surface Heat Flux during a Quench Operation, *Metallurgical and Materials Transactions B*, 36 (2005), 3, pp. 343-354
- [8] Dudas, J., Characterization and Avoidance of In-Field Defects in Solid-State Image Sensors. Ph. D. thesis, Simon Fraser University, Burnaby, Canada, 2008
- [9] Wang, F. Q., et al. Heat Transfer Analyses of Porous Media Receiver with Multi-Dish Collector by Coupling MCRT and FVM Method, *Solar Energy*, 93 (2013), July, pp. 158-168
- [10] Wang, F. Q., et al., Thermal Performance Analysis of Porous Media Receiver with Concentrated Solar Irradiation, *International Journal of Heat and Mass Transfer*, 62 (2013), July, pp. 247-254
- [11] Jones, T. E., et al., An Investigation of the Influence of Temperature on the Adsorption of the Chiral Modifier, (S)-Glutamic Acid, on Ni {111}, *Surface Science*, 587 (2005), 1, pp. 69-77

- [12] Liu, W., et al. Fast Dimensional Measurement Method and Experiment of the Forgings under High Temperature, *Journal of Materials Processing Technology*, 211 (2011), 2, pp. 237-244
- [13] Takeshi, M., et al. Evaluation of Heat Transfer Characteristics of Textile Goods by Infrared Image Measurement Method. *Journal of Textile Engineering*, 52 (2006), 1, pp. 37-41
- [14] Tank, V., et al., Multispectral Infrared Pyrometer for Temperature Measurement with Automatic Correction of the Influence of Emissivity, *Infrared Physics*, 30 (1990), 4, pp. 331-342
- [15] Li, Y., et al., Research on the Technique of Accurately Measuring Temperature with Infrared Thermal Imagers, *Proceedings*, 9<sup>th</sup> IEEE International Conference on Electronic Measurement & Instruments, Beijing, 2009, Vol. 4, pp. 573-578
- [16] Yang, Z., et al., Calculation of Infrared Temperature Measurement on Non-Lambertian Objects, *Spectroscopy and Spectral Analysis*, 30 (2010), 8, pp. 2093-2097
- [17] Qi, H., et al., A Modified Finite Volume Method for Simulating the Radiative Intensity in Any Specified Direction, *Proceedings*, 7<sup>th</sup> International Symposium on Heat Transfer, Beijing, 2008
- [18] Huang, Q. X., et al., Theoretical Fast Non-Intrusive 3-D Temperature Distribution Measurement within Scattering Medium from Flame Emission Image Analysis, *Optics Communications*, 292 (2013), Apr., pp. 25-30

